Genetic deletion of apolipoprotein A-I increases airway hyperresponsiveness, inflammation, and collagen deposition in the lung

Weiling Wang,[*,§§§,**] Hao Xu,[*,§§,***,†††] Yang Shi,[*,§§,***,†††] Sandhya Nandedkar,[§] Hao Zhang,[*,§§,***,†††] Haiqing Gao,[§§§,****] Thom Feroah,[**] Dorothee Weihrauch,[§,**,§§,***] Marie L. Schulte,[§,**,§§,***] Deron W. Jones,[*] Jason Jarzembowski,[††] Mary Sorci-Thomas,[††††] and Kirkwood A. Pritchard, Jr.[1,*,†,§§,***,†††]**

Departments of Surgery,[*] Pharmacology,[†] Anesthesiology,[§] Pediatrics,[**] Pediatric Pathology[††]; Cardiovascular Center[§§]; Translational Vascular Biology Program[***]; and Children's Research Institute,[†††] Medical College of Wisconsin, Milwaukee, WI; Department of Geriatrics,[§§§] Qilu Hospital, Shandong University, Jinan, China; Key Laboratory of Cardiovascular Proteomics of Shandong Province,[****] Jinan, Shandong, China; and Department of Pathology,[††††] Wake Forrest University School of Medicine, Winston-Salem, NC

Abstract **The relationship between high-density lipoprotein and pulmonary function is unclear. To determine mechanistic relationships we investigated the effects of genetic deletion of apolipoprotein A-I (apoA-I) on plasma lipids, paraoxonase (PON1), pro-inflammatory HDL (p-HDL), vasodilatation, airway hyperresponsiveness and pulmonary oxidative stress, and inflammation. ApoA-I null (*apoA-I*$^{-/-}$) mice had reduced total and HDL cholesterol but increased pro-inflammatory HDL compared with C57BL/6J mice. Although PON1 protein was increased in *apoA-I*$^{-/-}$ mice, PON1 activity was decreased. ApoA-I deficiency did not alter vasodilatation of *facialis* arteries, but it did alter relaxation responses of pulmonary arteries. Central airway resistance was unaltered. However, airway resistance mediated by tissue dampening and elastance were increased in *apoA-I*$^{-/-}$ mice, a finding also confirmed by positive end-expiratory pressure (PEEP) studies. Inflammatory cells, collagen deposition, 3-nitrotyrosine, and 4-hydroxy-2-nonenal were increased in *apoA-I*$^{-/-}$ lungs but not oxidized phospholipids. Colocalization of 4-hydroxy-2-nonenal with transforming growth factor β-1 (TGFβ-1 was increased in *apoA-I*$^{-/-}$ lungs. Xanthine oxidase, myeloperoxidase and endothelial nitric oxide synthase were increased in *apoA-I*$^{-/-}$ lungs. Dichlorodihydrofluorescein-detectable oxidants were increased in bronchoalveolar lavage fluid (BALF) in *apoA-I*$^{-/-}$ mice. In contrast, BALF nitrite+nitrate levels were decreased in *apoA-I*$^{-/-}$ mice. These data demonstrate that apoA-I plays important roles in limiting pulmonary inflammation and oxidative stress, which if not prevented, will decrease pulmonary artery vasodilatation and increase airway hyperresponsiveness.—**Wang, W., H. Xu, Y. Shi, S. Nandedkar, H. Zhang, H. Gao, T. Feroah, D. Weihrauch, M. L. Schulte, D. W. Jones, J. Jarzembowski, M. Sorci-Thomas, and K. A. Pritchard, Jr. **Genetic deletion of apolipoprotein A-I increases airway hyperresponsiveness, inflammation, and collagen deposition in the lung. *J. Lipid Res.* 2010.** 51: **2560–2570.**

Supplementary key words high-density lipoprotein • pro-inflammatory HDL • vasodilatation • xanthine oxidase • myeloperoxidase • 4-hydroxy-2-nonenal • 3-nitrotyrosine • TGFβ-1

Although apolipoprotein A-I (apoA-I), the major antiatherogenic apolipoprotein of HDL, is well recognized for protecting the heart against vascular disease, it also protects other vascular beds and organs. Recent studies provide new evidence supporting the notion that HDL plays a protective role in the lung. ABCA1, which interacts with lipid-poor apoA-I, was earlier shown to be essential for maintaining normal lipid composition and architecture of the lung as well as respiratory physiology (1). More recently, proteomic studies revealed that homozygous

This work was supported in part by National Institutes of Health Grants HL-081139 (K.A.P.), HL-079937 (K.A.P.), HL-49373 (M.S.T.), HL-64163 (M.S.T.), and HL-089779 (D.W.); by Pediatric Surgery Bridge Funding (K.A.P.); by National Natural Science Foundation of China Grant No. 30873145 (W.W. and H.G.); and by the China Scholarship Council (CSC) (W.W.). Its contents are solely the responsibility of the authors and do not necessarily represent the official views of the National Institutes of Health or other granitng agencies.

Manuscript received 18 December 2009 and in revised form 14 May 2010.

Published, JLR Papers in Press, May 14, 2010
DOI 10.1194/jlr.M004549

Abbreviations: apoA-I, apolipoprotein A-I; BALF, bronchoalveolar lavage fluid; p-HDL, pro-inflammatory HDL; 4-HNE, 4-hydroxynonenal; MPO, myeloperoxidase; eNOS, endothelial nitric oxide synthase; 3-NT, 3-nitrotyrosine; PEEP, positive end-expiratory pressure; PON1, paraoxonase; TGFβ-1, transforming growth factor β-1; XO, xanthine oxidase.

[1]To whom correspondence should be addressed.
e-mail: kpritch@mcw.edu

sickle cell anemia patients with pulmonary arterial hypertension (PAH) consistently had lower apoA-I levels than sickle patients without PAH (2). Interestingly, genetic deletion of endothelial lipase resulted in a nearly 2-fold increase in HDL, which was credited with decreasing airway hyperresponsiveness and pulmonary inflammation in ovalbumin (OVA)-sensitized BALB/c mice (3). Although these reports provide some support for the idea that HDL helps maintain healthy lungs, no studies have directly determined the effects of apoA-I, or lack thereof, on pulmonary inflammation, vasodilatation, and airway hyperresponsiveness.

Increasing evidence suggests that elevated levels of HDL are not always atheroprotective (4–7). Indeed, chronic states of inflammation and oxidative stress have been shown to convert HDL from an anti-inflammatory and anti-atherogenic lipoprotein into a pro-inflammatory and pro-atherogenic lipoprotein, making it useless for protecting the vessel wall against the effects of atherogenic concentrations of LDL (8). Asthma also increases inflammation and oxidative stress (9–12). Such inflammatory changes may explain why adult-onset asthma is associated with significant increases in carotid artery intimal-medial thickness in women (13). In this article we examine the effects of genetic deletion of apoA-I on pulmonary inflammation, vasodilatation, collagen deposition, and airway hyperresponsiveness. Our findings suggest that apoA-I plays a critical role in protecting pulmonary artery and airway function as well as preventing inflammation and collagen deposition.

MATERIALS AND METHODS

Mice

Male *apoA-I*$^{-/-}$ (B6.129P2-*Apoa1*^{tm1Unc}/J; SN 002055, which is on a C57BL/6J genetic background) and C57BL/6J (SN 000664) mice were purchased from Jackson Laboratory (Bar Harbor, ME) at 8 weeks of age. Mice were housed in sterile autoclavable microisolation cages with 12 h dark and light cycles, free access to water, and standard chow diet. At 16 weeks of age, mice were either anesthetized for airway hyperresponsiveness or euthanized by intraperitoneal injection of Nembutal prior to collection of plasma, bronchial lavage fluid (BALF), or tissues. The Institutional Animal Care and Use Committee (IACUC) of Medical College of Wisconsin approved all animal protocols used in the study.

Plasma total cholesterol, HDL cholesterol, and pro-inflammatory HDL

Blood was collected in sodium heparin via left cardiac puncture and then centrifuged to harvest plasma, which was aliquoted and frozen at −80°C until analysis. Total cholesterol (TC) was quantified using a cholesterol oxidase/esterase kit from Wako Chemical, Inc. (Richmond, VA). HDL was isolated from whole plasma with a solution of dextran-sulfate-$MgCl_2$ (10 g/l, 0.5 M) (Berkeley HeartLab Inc., Alameda, CA), which precipitates apoB-containing lipoproteins. HDL cholesterol was quantified using a HDL Cholesterol E kit from Wako Diagnostics. Pro-inflammatory HDL (p-HDL) was determined using a modified method of a previously published cell-free assay (14). Briefly, HDL was incubated with $CuCl_2$ (5 μmol/l, final concentration) for 1 h at 37°C in a 384-well microtiter plate (MJ Research Inc., Waltham, MA). After incubation, 10 μl of 2′,7′-dichlorodihdrofluorescein (H_2DCF) solution (0.2 mg/ml) was added to the HDL-Cu^{2+} mixture in a total volume of 50 μl. Rates of fluorescence (Ex, 485 nm; Em, 530 nm) were determined over the next 2 h at 30 min intervals using a Spectra Max Gemini EM fluorescence plate reader (Molecular Devices, Sunnyvale, CA).

Plasma PON1 arylesterase activity

Arylesterase activity of paraoxonase (PON1) was performed on whole plasma using phenyl acetate as the substrate as described (15). Initial rates of hydrolysis were determined spectrophotometrically at 270 nm on DU® 640 spectrophotometer (Beckman Coulter® Instruments, Brea, CA). An aliquot of 20 μl of 30× diluted mouse plasma was added to a final reaction volume of 500 μl (phenyl acetate [100 mmol/l] and $CaCl_2$ [100 mmol/l] in Tris-HCl [40 mmol/l] buffer, pH 8.0) for 6 min at 25°C. Rates of spontaneous hydrolysis of phenyl acetate over the same time period were subtracted as blank. The extinction coefficient at 270 nm for phenyl acetate is 1310 $mol \bullet l^{-1} \bullet cm^{-1}$. One unit of arylesterase activity equals 1 μmole of phenyl acetate hydrolyzed per ml per min.

Quantification of plasma nitrite+nitrate

Nitrite+nitrate concentrations were determined by ozone chemiluminescence using the NO Analyzer (Model 280i, GE Analytical-Sievers, Boulder, CO) as described (16, 17). An aliquot of 30 μl was injected (plasma was diluted by 1:30) into a sealed glass reaction chamber at 95°C containing VCl_3 (17). Nitric oxide chemiluminescence signals were quantified and peak areas compared with the areas of external nitrate standards. Results are expressed in μM.

Estimates of plasma 3-nitrotyrosine

An aliquot of plasma from C57BL/6J and *apoA-I*$^{-/-}$ mice was pipetted onto nitrocellulose membranes and allowed to bind. Membranes were blocked with 5% nonfat dry milk dissolved in fresh PBS-Tween (0.1%) and then incubated overnight at 4°C with antibodies for 3-nitrotyrosine (3-NT, 1:5000; Millipore, Billerica, MA). The next day, the membranes were washed and incubated with the appropriate HRP-conjugated secondary antibody for 1 h. Bands of identity were visualized with ECL chemiluminescence (GE Healthcare, Piscataway, NJ) following the manufacturer's recommendations. Autoradiograms were scanned with a laser densitometer or a UMax scanner. Dot blot densities were quantified using UN-SCAN-IT Gel 6.1 Software (Silk Scientific, Orem, UT).

Effects of genetic deletion of apoA-I on vasodilatation

Facialis and pulmonary arteries were isolated from C57BL/6J and *apoA-I*$^{-/-}$ mice by microdissection as previously described (14). Vasodilatation of pressurized (60 cm of H_2O) *facialis* arteries was examined in the absence and presence of L-nitroargininemethylester (L-NAME; 200 μM, final concentration) as previously described (14). Changes in pulmonary artery tension in response to acetylcholine (ACh) were recorded on a DMT wire-myograph using protocols similar to that previously described (18).

Measurements of lung mechanics

Mice (mean age = 15–16 weeks) were anesthetized with sodium pentobarbital (90 mg/kg) and placed on a heated surgical pad set at a constant temperature of 37°C. Mice were tracheostomized with an 18-gauge cannula and mechanically ventilated in a quasi-sinusoidal fashion with a small animal ventilator (flexiVent, SCIREQ, Montreal, PQ, Canada) at 150 breaths per minute (19) and a tidal volume (V_T) of 10 ml × kg^{-1} body weight. To eliminate involuntary smooth muscle cell contraction during

airway studies and to ensure paralysis during lung mechanic studies, 10 mg/kg gallamine triethiodide (Sigma-Aldrich, St. Louis, MO) was injected IP.

After one 1 min of regular ventilation with positive end-expiratory pressure (PEEP) set at 3 cm H_2O, the lung volume history was standardized by two deep inspirations, delivered over 6 s at constant flow with a pressure limit of 30 cm H_2O, followed by 5 min of regular ventilation. Basal respiratory system impedance (*Zrs*) was then assessed using the forced oscillation technique (FOT) applied over 2 s (a Prime-2 perturbation) using the flexiVent system. Then, following a 60 s period of default ventilation, a series of challenges were performed at different levels of PEEP: 0, 3, 6, and 9 cm H_2O. Each level of PEEP was held for 80 s with the Prime-2 perturbation repeated twice, once at 35 s and the other at 70 s Measurements at each PEEP were repeated twice, and the parameter estimates from each of the signal applications averaged and logged.

Methacholine challenge

Airway hyperresponsiveness was then assessed by administering series of progressively increasing concentrations of methacholine (MCh) to induce successive increases in bronchoconstriction. PEEP was set at 3 cm H_2O for the MCh studies. Mice were challenged with 70 μl of MCh (Sigma-Aldrich) of increasing concentrations (3.125–100 mg/ml). MCh aerosols were generated using an ultrasonic nebulizer (DeVilbiss LtraNeb 2000, Somerset, PA, USA) and delivered to the inspiratory line of the ventilator using room air. Each aerosol was delivered for 30 s, during which time ventilation was maintained mechanically by the flexiVent. Immediately following MCh delivery, the Aeroneb nebulizer was quickly removed from the inspiratory arm of the flexiVent system and default ventilation was reinstated. Then for the next 3 min, each aerosol was delivered for 30 s, during which time regular ventilation was maintained. A Prime 2- perturbation was applied every 20 s (by the flexiVent) and changes in respiratory impedance (*Zrs*) in response to each MCh dose was determined using force oscillation techniques (FOT) generated by the flexiVent.

Briefly, the pressure and flow data obtained during Prime-2 perturbations were used by the flexiVent to calculate *Zrs*, which was then fit to a model consisting of a single airway serving a constant-phase viscoelastic tissue unit (19, 20).

$$\mathrm{Zrs}(f) = \mathrm{R_N} + i2\pi f\,\mathrm{law} + \frac{\mathrm{G} - i\mathrm{H}}{(2\pi f)^{\alpha}} \qquad (Eq.\,1)$$

In this model equation, R_N is Newtonian resistance composed mostly of the flow resistance of the conducting pulmonary airways, Iaw reflects the inertance of the gas in the central airways (this can be ignored in mice below a breathing frequency of 20 Hz (21), G reflects tissue resistance, viscous dissipation of energy in the parenchymal respiratory tissues (20), H reflects elastic energy storage in the tissues (tissue stiffness), f is frequency $i = \sqrt{-1}$, and α couples G and H in the following equation (20).

$$\alpha = \frac{2}{\pi}\tan^{-1}\frac{\mathrm{H}}{\mathrm{G}} \qquad (Eq.\ 2)$$

This model has been shown to accurately describe respiratory impedance both under control conditions and during mild bronchoconstriction (21–23). The advantage of this model is that it allows for a better distinction between central and peripheral airway changes in the lung.

Histology

A 0.5 ml aliquot of zinc-formalin was used to inflate the lung prior to removal. The lung was fixed in zinc-formalin, embedded in paraffin, sectioned, and then stained with hematoxylin and eosin (H and E) for histology or with McLetchie's trichrome to assess collagen deposition.

Isolation of BALF and analysis

After exsanguination, the tracheas of C57BL/6J and apoA-I/ mice were cannulated with polyethylene tubing. BALF was obtained by flushing the lung with PBS, first 1 ml followed by 0.5 ml. The rinses were combined, and the BALF was centrifuged at 2000 rpm for 10 min at 4°C. The supernatant was removed and stored at −80°C. The cell pellet was gently resuspended in 1 ml PBS. An aliquot of 500 μl was used to prepare slides using a Cytospin (Model2; Shandon Scientific Co., Pittsburg, PA). Differential cell counts were made from slides stained with Diff-Quick. Five hundred cells were counted and identified (magnification 40×) for each mouse by a pathologist who had no prior knowledge of slide identities. The remainder of the cell suspension was centrifuged again, and the pellet was stored at −80°C until further analysis.

Immunofluorescence

Three C57BL/6J and *apoA-I*$^{-/-}$ mice were anesthetized and euthanized by exsanguination. The lungs were harvested, fixed in zinc-formalin, and embedded in paraffin. Sections were chosen at random by a technician who had no prior knowledge concerning slide identity. Immunofluorescence was performed on 5 μm sections of paraffin-embedded, PBS-zinc-formalin–fixed lungs. Two sections were present on each slide. Sections were deparaffinized with xylene and rehydrated in a descending alcohol row (from 95% to 50%). The sections were incubated separately with antibodies against 3-NT (24), anti-T15 autoantibodies (anti-T15 antibodies were prepared from hybridoma cells, which were kindly provided by Dr. J. F. Kearney, University of Alabama, Burmingham, AL) as previously described (25), anti-4-hydroxynonenal (4-HNE) Michael's adducts antibody (Calbiochem-EMD, LaJolla, CA), or with transforming growth factor β-1 (TGFβ-1) antibody (Santa Cruz Biotechnology, Santa Cruz, CA) for colocalization studies. Slides were washed with PBS (3×) and then incubated with the appropriate secondary antibodies. The slides were washed and sealed under cover slips. Images were captured using a krypton argon laser Nikon Eclipse TE2000U confocal microscope (Melville, NY) with 10×/0.17 aperture objective. Total magnification was 100 with Ex/Em at 488/580 nm for Alexa 488 and 633/661 nm for TO-PRO-3. Images were captured (10/lung section; 2 sections per slide for a total of 60 images per test group) and analyzed using IBM EZC1 software (Armonk, NY). Controls for staining were slides incubated in the absence of primary antibodies.

Western blot analysis

Frozen lungs were pulverized in a stainless steel mortar and pestle that were prechilled with liquid nitrogen. The powder was quickly transferred into a 50 ml conical tube, homogenized in MOPS buffer with Polytron^{R} (PT 1200E, Kinematica, Switzerland), and the homogenate was centrifuged at 13000 rpm (at 4°C for 10 min). Protein concentrations were quantified using BCA reagent.

An aliquot of 60 μg protein was mixed with 5× Laemmle buffer and denatured by heating at 95°C for 5 min. For plasma protein estimates, gels were loaded with 3 μl of plasma. Proteins were separated by SDS-PAGE (4–20%, Bio-Rad) and transferred onto nitrocellulose membranes. Membranes were blocked with 5% nonfat dry milk dissolved in fresh PBS-Tween (0.1%) and then incubated overnight at 4°C with antibodies for xanthine oxidase (XO, 1:500; Lab Vision Corporation, Freemont, CA), myeloperoxidase (MPO, 1:1000; Millipore, Billerica, MA), or endothelial nitric oxide synthase (eNOS, 1:10,000; Santa Cruz Biotechnology, Santa Cruz, CA). The next day, the membranes were washed

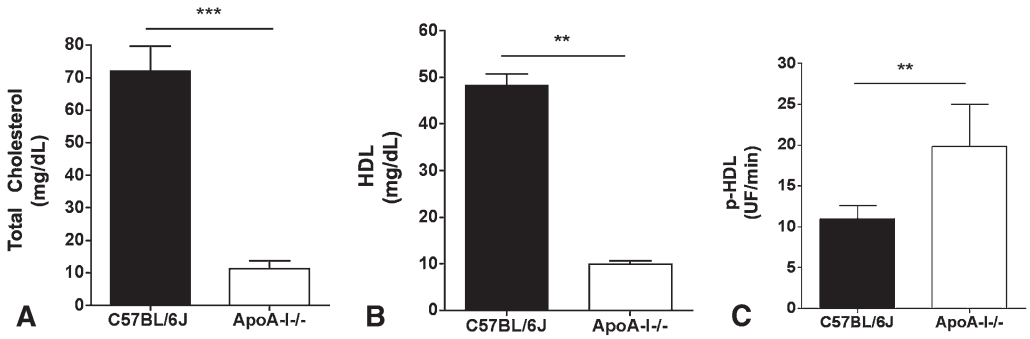

Fig. 1. Plasma total cholesterol, HDL cholesterol, and pro-inflammatory HDL. Bar graphs showing that *apoA-I*$^{-/-}$ mice (n = 5) had reduced levels of plasma total cholesterol (A) and HDL cholesterol (B) compared with control C57BL/6J mice (n = 7). However, HDL in *apoA-I*$^{-/-}$ mice (n = 5) contained higher p-HDL (C) levels compared with control C57BL/6J mice (n = 7). ** = $P < 0.01$, *** = $P < 0.001$. apoA-I, apolipoprotein A-I; p-HDL, pro-inflammatory HDL.

and incubated with the appropriate HRP-conjugated secondary antibody for 1 h. Bands of identity were visualized with ECL chemiluminescence (GE Healthcare, Piscataway, NJ) following the manufacturer's recommendations. Autoradiograms were scanned with a laser densitometer or an UMax scanner. Band densities were quantified using UN-SCAN-IT Gel 6.1 Software (Silk Scientific, Orem, UT).

BALF DCF-detectable oxidants

Oxidation of H_2DCF was used to obtain an index of the levels of oxidants in BALF. An aliquot of BALF (75 μl) was mixed with H_2DCF (100 μl PBS + 25 μl H_2DCF [a 1 × 10 dilution of 2 mg/ml] in a total volume of 200 μl) and this mixture incubated for 2 h at 37°C. Absolute changes in fluorescence (Ex 485 nm; Em 530 nm) were determined at the end of the 2 h incubation period using Spectra Max Gemini EM fluorescence plate reader (Molecular Devices, Sunnyvale, CA).

Statistical analysis

Data are presented as mean ± SEM. Results were analyzed by Student's *t*-test, Mann-Whitney test, or Fisher's exact test where appropriate. Airway and pulmonary artery ring data were analyzed by 2-way ANOVA to determine significance between curves and a Bonferroni posttest to determine significance of points between the curves. All statistical analysis was performed using Graph Pad Prism Software (version 5.0).

RESULTS

Effects of apoA-I deficiency on lipids and oxidative stress

ApoA-I$^{-/-}$ mice had reduced levels of plasma total cholesterol and HDL cholesterol compared with control mice (**Fig. 1A**, B). Although *apoA-I*$^{-/-}$ mice contained less HDL than control mice, their HDL oxidized at a faster rate than HDL from control mice, indicating that HDL in *apoA-I*$^{-/-}$ mice was pro-inflammatory (26) (Fig. 1C). PON1 plasma protein in a*poA-I*$^{-/-}$ mice was increased compared with protein levels in C57BL/6J mice (**Fig. 2A**, B). However, PON1 activity was decreased (≈34%, $P < 0.001$) compared with controls (Fig. 2C). Although the concentration of plasma nitrite+nitrate was decreased in *apoA-I*$^{-/-}$ mice, plasma 3-NT levels were increased compared with the levels in control mice (**Fig. 3A** and B, respectively).

Effects of apoA-I deficiency on vasodilatation

Studies on ACh-dependent vasodilatation of isolated and pressurized *facialis* arteries revealed that genetic loss of apoA-I had no effect on relaxation responses in these vessels (**Fig. 4A** versus B). These observations are consistent with previous studies showing that *apoA-I*$^{-/-}$ mice are not more susceptible to atherosclerosis (27, 28). However, relaxation responses of pulmonary artery (PA) rings isolated from *apoA-I*$^{-/-}$ mice were impaired at the highest

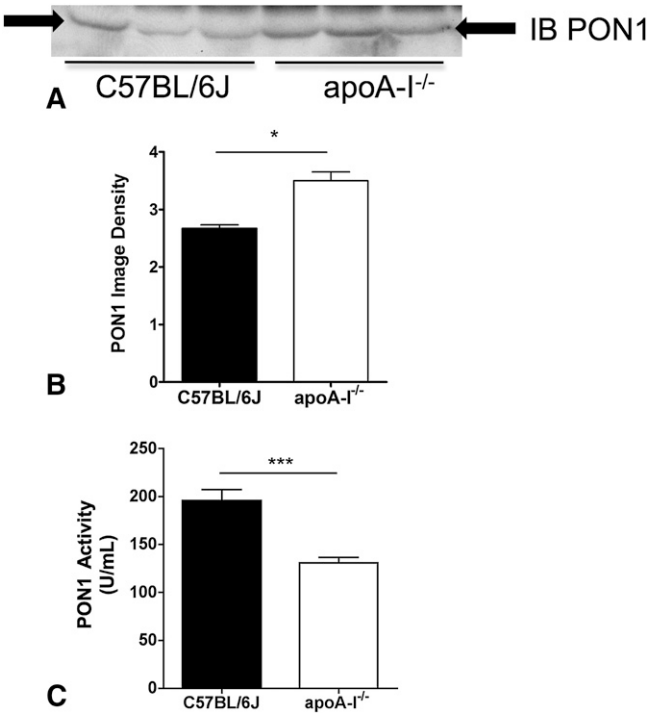

Fig. 2. Plasma PON1 expression and activity. Autoradiograms of PON1 protein expression and bar graphs showing relative band densities. *ApoA-I*$^{-/-}$ mice had increased plasma protein levels of PON1 but reduced PON1 activity (≈34%) compared with control C57BL/6J mice. A: Representative images of autoradiograms of PON1 protein in murine plasma. B: Relative densitometry in arbitrary units of autoradiograms of PON1 (n = 3). C: PON1 arylesterase activity of plasma samples from C57BL/6J (n = 7) and *apoA-I*$^{-/-}$ mice (n = 6). *$P < 0.05$, ***$P < 0.001$. apoA-I, apolipoprotein A-I; PON1, paraoxonase.

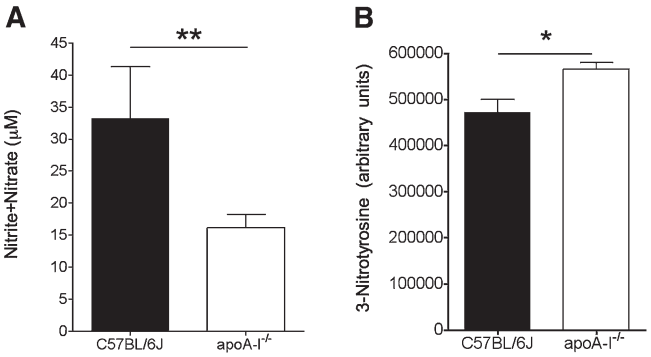

Fig. 3. Plasma nitrite+nitrate concentrations and 3-NT formation. A: Bar graphs showing that plasma nitrite+nitrate concentrations in *apoA-I*$^{-/-}$ mice (n = 6) are reduced compared with concentrations in C57BL/6J mice (n = 7). B: Bar graphs showing relative changes in densities of autoradiograms of 3-NT in plasma from C57BL/6J (n = 7) and *apoA-I*$^{-/-}$ mice (n = 6). *$P < 0.05$, **$P < 0.01$. apoA-I, apolipoprotein A-I; 3-NT, 3-nitrotyrosine.

ACh concentration (Fig. 4C). Two-way ANOVA (ANOVA) was performed on these data to determine whether mouse strain had any influence. Although on a concentration basis, the major difference in the curves was at the highest ACh concentration, two-way ANOVA indicated that that the strain of mouse (C57BL/6J versus *apoA-I*$^{-/-}$ mice) influenced the shape of the curves and that the curves were "extremely" significantly different ($P < 0.0004$). The importance of this analysis is that there is less than a 0.044% chance of these curves occurring by random events. The sudden decrease in vasodilatation by the *apoA-I*$^{-/-}$ PA rings means that the *apoA-I*$^{-/-}$ PA rings are actually contracting in response to the highest dose of ACh. In contrast, PA rings isolated from control mice continued to vasodilate. This change in vasodilatory response is an important phenotypic change and, to our knowledge, the first demonstration that genetic loss of apoA-I specifically alters pulmonary vascular physiology. Such changes in the physiological responses of pulmonary arteries in *apoA-I*$^{-/-}$ mice are consistent with the idea that chronic exposure to inflammation and oxidative stress impair vasodilatation.

Effects of apoA-I deficiency on airway hyperresponsiveness

The flexiVent provides quantitative information regarding the mechanical properties of the entire airway tree. In the large airways it assesses Newtonian resistance (R_N), while in the smaller airways it is able to determine changes in tissue damping (G) and tissue elastance (H). In both *apoA-I*$^{-/-}$ and C57BL/6J mice, methacholine (MCh) induced dose-dependent increases in airway resistance associated with tissue dampening (G) ($P < 0.01$; **Fig. 5B**) and tissue elastance (H) ($P < 0.001$; Fig. 5C), but not R_N (Fig. 5A). Effects of increasing PEEP on airway mechanical parameters, R_N, G and H, are shown in Figs. 5D, 4E, and 4F, respectively. G was increased in *apoA-I*$^{-/-}$ mice compared with control mice at baseline PEEP = 0 ($P < 0.01$) as well as throughout the entire PEEP curve ($P < 0.001$). H was increased in *apoA-I*$^{-/-}$ mice compared with controls throughout the entire PEEP range ($P < 0.001$).

Effects of apoA-I deficiency on histology

H and E sections of lungs harvested from a*poA-I*$^{-/-}$ mice (**Fig. 6A**, two lower-left images) contained twice the number of leukocytes than lungs from C57BL/6J mice (Fig. 6A, B, one upper-left image, $P < 0.025$, 2-tailed Student *t*-test). The cell counts in sections of lung isolated from *apoA-I*$^{-/-}$ mice were composed predominantly of neutrophils, leukocytes, and eosinophils. In contrast, the cell counts in sections of lungs isolated from C57BL/6J mice contained an occasional neutrophil. Although inflammatory cells in the lungs are increased by the absence of apoA-I, the number of pro-inflammatory cells per high powered field in these mice is much lower than that in OVA-sensitized mice. OVA sensitization often increases leukocyte infiltration in the lung as high as 25–50 cells per HPF (29). Sections of lungs harvested from

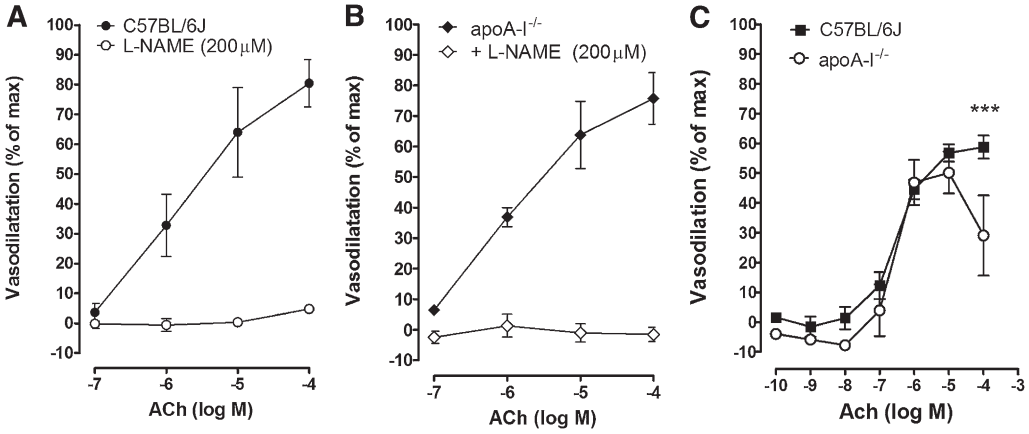

Fig. 4. Vasodilatation of *facialis* and pulmonary arteries. Line graphs showing that vasodilatation of isolated and pressurized facialis arteries from C57BL/6J and *apoA-I*$^{-/-}$ mice dilate to the same extent when stimulated with increasing doses of ACh. A: n = 5. B: n = 3. Statistical analysis C57BL/6J versus *apoA-I*$^{-/-}$ (P = NS). C: Line graph showing that vasodilatation of pulmonary artery rings is slightly impaired in *apoA-I*$^{-/-}$ mice compared with control C57BL/6J mice especially at the highest ACh concentration tested (n = 7, C57BL/6J and n = 4, *apoA-I*$^{-/-}$ mice; ***$P < 0.001$). Ach, acetylcholine; apoA-I, apolipoprotein A-I; L-NAME, L-nitroargininemethylester.

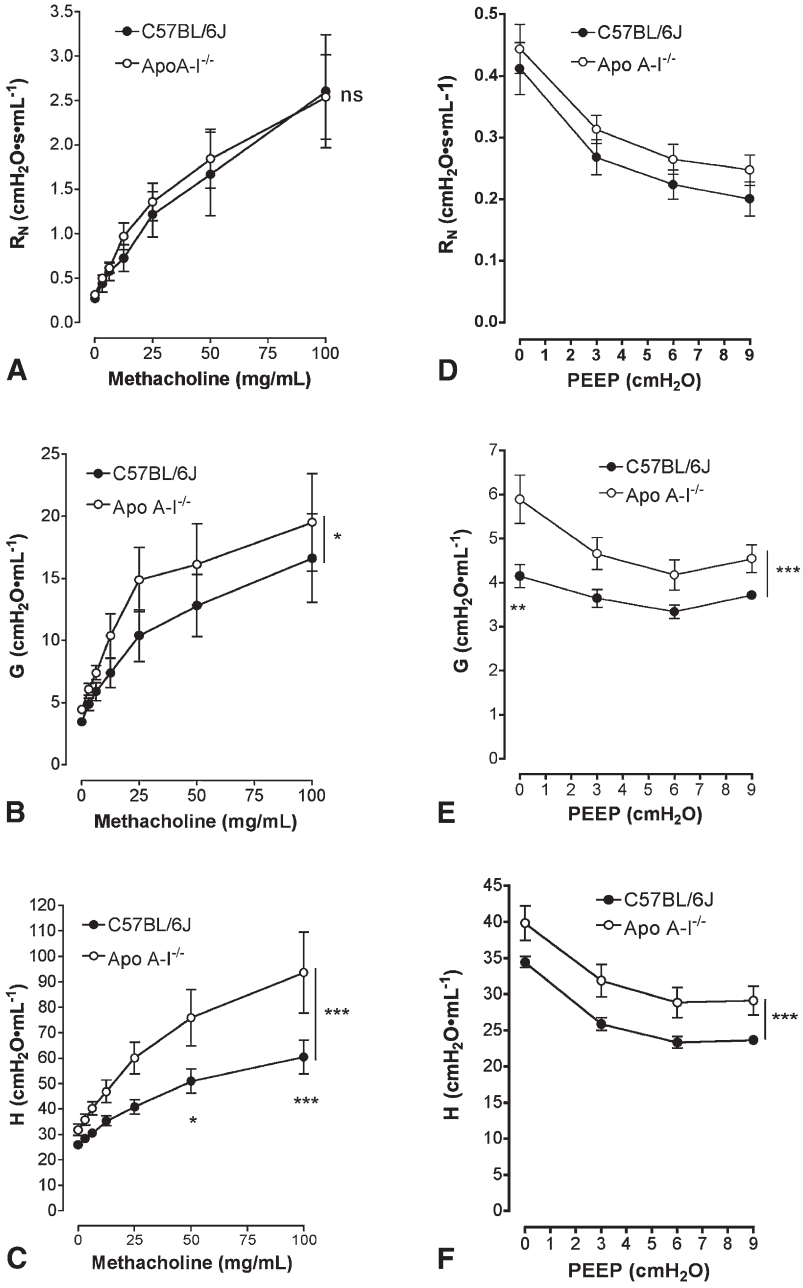

Fig. 5. Airway mechanics. Line graphs showing that airway resistance to MCh challenge is increased in apoA-I-deficient mice with respect to (B) tissue damping (G, n = 5–7) and (C) tissue elastance (H, n = 5–7) but not with respect to physiological responses of (A) large airways (R_N, n = 5–7, NS) and that airway responses to increasing PEEP levels are increased in *apoA-I*$^{-/-}$ mice compared with C57BL/6J mice with respect to (E) tissue damping (G, n = 7) and (F) tissue elastance (H, n = 7) but not with respect to (D) large airways (R_N, n = 7). $^{*}P < 0.05$, $^{**}P < 0.01$, $^{***}P < 0.001$. apoA-I, apolipoprotein A-I; MCh, methacholine; PEEP, positive end-expiratory pressure.

apoA-I$^{-/-}$ mice also revealed increased collagen deposition (Fig. 6A, two lower-right images). Trichrome staining is stronger and more extensive in *apoA-I*$^{-/-}$ sections than in sections of lungs from C57BL/6J mice (Fig. 6A, upper-right image). Cytospins of BALF isolated from *apoA-I*$^{-/-}$ and C57BL/6J mice showed that the BALF contained predominately alveolar macrophages (>98%). Cytospins of BALF isolated from C57BL/6J and *apoA-I*$^{-/-}$ mice reveal that the genetic loss of apoA-I did not have significant effect on lymphocyte infiltration in the bronchoalveolar space (Fig. 6C).

Effects of apoA-I deficiency on biomarkers of oxidative stress and inflammation

Immunofluorescence studies revealed that lung sections from *apoA-I*$^{-/-}$ mice stained stronger for 3-NT and 4-HNE Michael's adducts than sections from controls (**Fig. 7A**, B). In contrast to these two biomarkers of oxidative stress, no differences were observed for immunofluorescent staining for T15-type autoantibodies between *apoA-I*$^{-/-}$ and control mice (Fig. 7A). Genetic loss of apoA-I increases colocalization of 4-HNE-derived Michael's adducts with active TGFβ-1 in pulmonary airways (Fig. 7B). Lungs from *apoA-I*$^{-/-}$ mice express higher levels of XO, MPO, and eNOS than lungs from C57BL/6 mice (**Fig. 8**). These data are in contrast to nitrite+nitrate data showing that BALF isolated from *apoA-I*$^{-/-}$ mice contains less nitrite+nitrate than BALF isolated from C57BL/6J mice (**Fig. 9A**). Finally, BALF from *apoA-I*$^{-/-}$ mice increased DCF fluorescence to a greater extent than BALF from C57BL/6J mice (Fig. 9B). These data indicate that BALF from *apoA-I*$^{-/-}$ mice contains more pro-oxidant compounds than BALF from C57BL/6J mice.

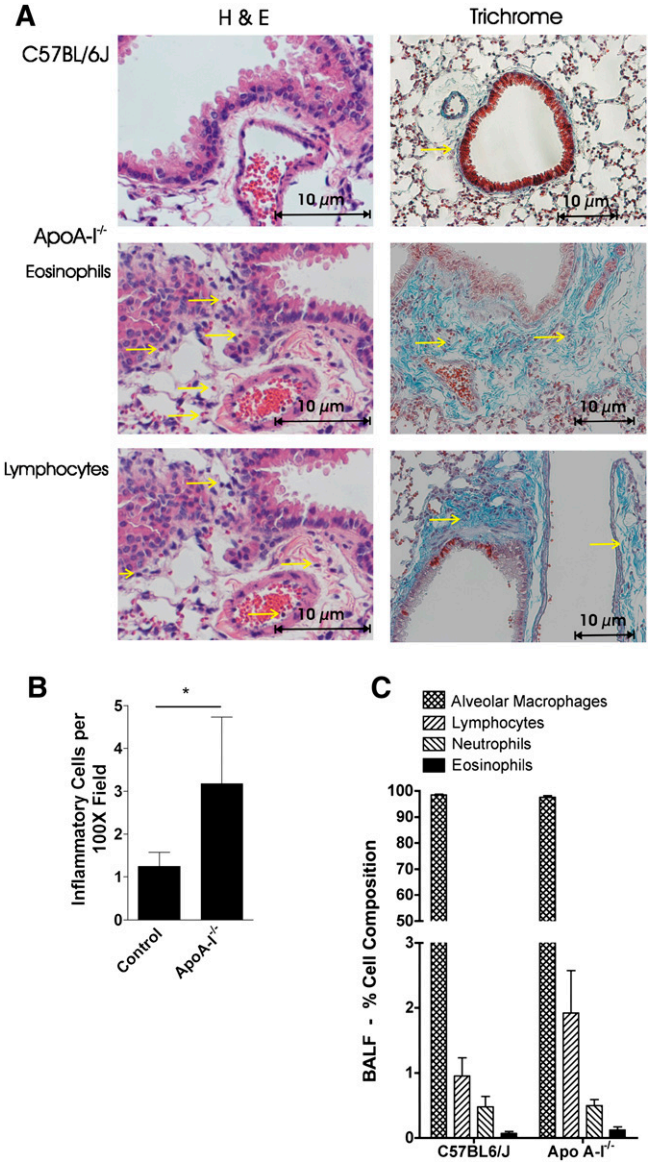

Fig. 6. Histology and BALF cells. A: H and E images (40×) of lungs from *ApoA-I*$^{-/-}$ mice appear to contain more inflammatory cells in perialveolar and perivascular regions (lower left). Trichrome images (20×) show that *apoA-I*$^{-/-}$ mice have higher levels of collagen deposition (lower right) than lungs from C57BL/6J mice (upper left and upper right, respectively). B: Cell counts per high power field (100×, oil immersion). C: Composition of inflammatory cells in BALF from a*poA-I*$^{-/-}$ mice (n = 12) compared with the composition of cells in BALF from C57BL/6J mice (n = 11). apoA-I, apolipoprotein A-I; BALF, bronchoalveolar lavage fluid; H and E, hematoxylin and eosin.

DISCUSSION

The role of apoA-I in pulmonary inflammation and airway hyperresponsiveness was investigated in mice that were genetically engineered to be deficient in apoA-I. Genetic loss of apoA-I in mice resulted in changes in lung histology and airway physiology that are consistent with the idea that apoA-I plays an important anti-inflammatory role in the lung.

Deletion of apoA-I altered plasma lipoprotein profiles by decreasing total cholesterol and HDL cholesterol (Fig. 1A, B), confirming previous reports (27, 28). Although it has long been known that HDL is decreased in *apoA-I*$^{-/-}$ mice, we report here that the levels of pro-inflammatory HDL are also increased (Fig. 1C). This observation is consistent with our previous report examining the effects of a genetic loss of apoA-I on pro-inflammatory HDL in *Ldlr*$^{-/-}$*/apoA-I*$^{-/-}$ mice relative to levels in *Ldlr*$^{-/-}$ mice (14). The cell-free assay for quantifying pro-inflammatory HDL is a convenient means for determining whether HDL isolated from a group of patients, different strains of mice or experimental test groups is more easily oxidized than HDL isolated from controls. We and others have shown that pro-inflammatory HDL levels are increased in diseases characterized by chronic states of oxidative stress (25, 30, 31). This increase in pro-inflammatory HDL in the *apoA-I*$^{-/-}$ mice coincides with a decrease in PON1 activity even though PON1 protein levels were actually increased (Fig. 2). The lower PON1 activity levels in the *apoA-I*$^{-/-}$ mice are consistent with the fact that PON1 can be inactivated by chronic increases in oxidative stress (32). These data provide additional evidence that *apoA-I*$^{-/-}$ mice experience more oxidative stress than C57BL/6J mice.

Although plasma from the *apoA-I*$^{-/-}$ mice contained less nitrite+nitrate, than plasma from C57BL/6J mice, it also contained a modest, but statistically significant increase in 3-nitrotyrosine (3-NT) (Fig. 3). This significant increase in 3-NT, a biomarker of oxidative stress, provides a third level of support for the idea that *apoA-I*$^{-/-}$ mice experience greater oxidative stress than C57BL/6J mice. Interestingly, although *apoA-I*$^{-/-}$ mice had lower levels of HDL and increased plasma 3-NT, peripheral vascular function in *apoA-I*$^{-/-}$ mice was unaffected compared with controls (Fig. 4). We have shown before that ACh-dependent vasodilatation of *facialis arteries* is endothelial nitric oxide synthase-dependent (14). The observations here are consistent with previous studies showing that *apoA-I*$^{-/-}$ mice are not more susceptible to atherosclerosis (27, 28). Although genetic loss of apoA-I did not impair vasodilatation in *facialis* arteries (Fig. 4A, B), it did alter the relaxation responses of pulmonary artery rings (Fig. 4C). At 10^{-4} M ACh, C57BL/6J pulmonary rings continue to vasodilatate; however, rings from *apoA-I*$^{-/-}$ mice actually constrict when treated with 10^{-4} M ACh. These data are consistent with the idea that the oxidative stress and/or inflammation associated with loss of apoA-I impairs pulmonary vascular function (25, 33).

Genetic loss of apoA-I also increased airway hyperresponsiveness, collagen deposition, and biomarkers of oxidative stress in the lungs. Methacholine is a bronchoconstrictor used clinically to assess airway responses in patients suspected of having asthma. Inspiration of nebulized methacholine increases bronchoconstriction which in turn increases airway resistance. Measurements of airway resistance after inspiration of methacholine provide a sensitive means of determining whether airway physiology is impaired. Using force oscillatory techniques, changes in airway resistance can be assessed not only in the central

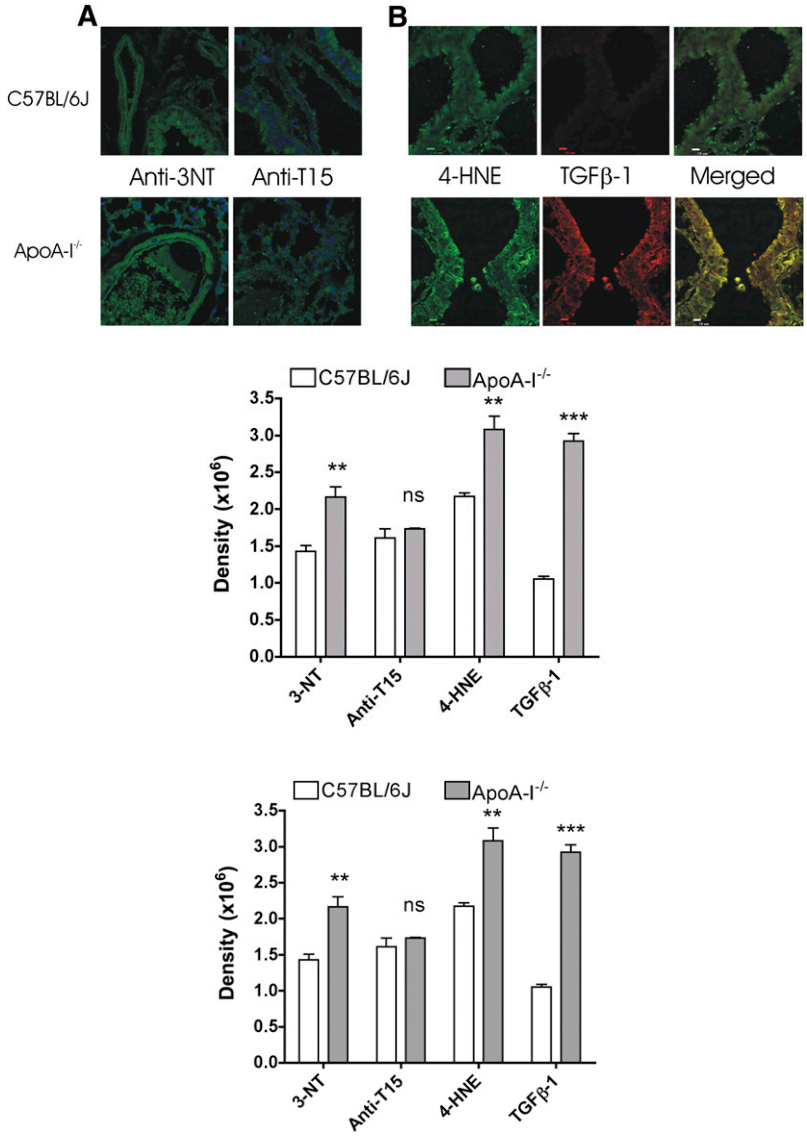

Fig. 7. Biomarkers of oxidative stress and TGFβ-1 activation. A: Immunofluorescence of lung sections from *apoA-I*$^{-/-}$ mice contained increased levels of 3-NT (green) and 4-HNE but not anti-T15 autoantibodies (green) than sections of lungs from C57BL/6J mice. Nuclei of cells are counterstained with ToPro-3 (blue). B: Immunofluorescence and colocalization of 4-HNE Michael's adducts (green) and TGFβ-1 (red) are increased in sections of lungs isolated from *apoA-I*$^{-/-}$ mice and compared with sections of lungs isolated from C57BL/6J mice. Nuclei of cells are counterstained with ToPro-3 (blue). Total magnification was 100×. C: Fluorescent images (10/lung) were captured using a confocal microscope. Sections were chosen at random by a technician who had no prior knowledge concerning slide identity. Ten images were analyzed per section for a total of 60 images for each test group. Average ± SEM of image densities for green and red in the sections is provided in the bar graph. apoA-I, apolipoprotein A-I; 4-HNE, 4-hydroxynonenal; 3-NT, 3-nitrotyrosine; TGFβ-1, transforming growth factor β-1.

airways (R_N) but also in the lung parenchyma with respect to tissue dampening (G) or elastance (H). Our studies showed that genetic loss of apoA-I had little effect on central airway resistance (R_N), but it did increase resistance with respect to G and H (Fig. 5). G reflects changes in either the physical properties of pulmonary tissues or regional heterogeneity related to tissue damping (19). H is a parameter indicative of lung elastance or the ability of the lungs to recoil after expansion resulting from inspiration. Accordingly, an increase in G would most likely reflect airway closure due to liquid bridges forming within the small airways and alveoli (contributing to increased G), whereas chronic changes in H would most likely reflect changes in the intrinsic mechanical properties of the lung parenchyma (19, 34–36). Increases in G and H in response to a bronchoconstrictor are consistent with our histology studies showing that collagen deposition is greater in *apoA-I*$^{-/-}$ mice than C57BL/6J mice (Fig. 6). Histological studies revealed that there were more inflammatory cells in the lungs of *apoA-I*$^{-/-}$ mice than in C57BL/6J mice. The number of cells in the lungs of these mice is low in comparison to ovalbumin-sensitized mice in which very high numbers

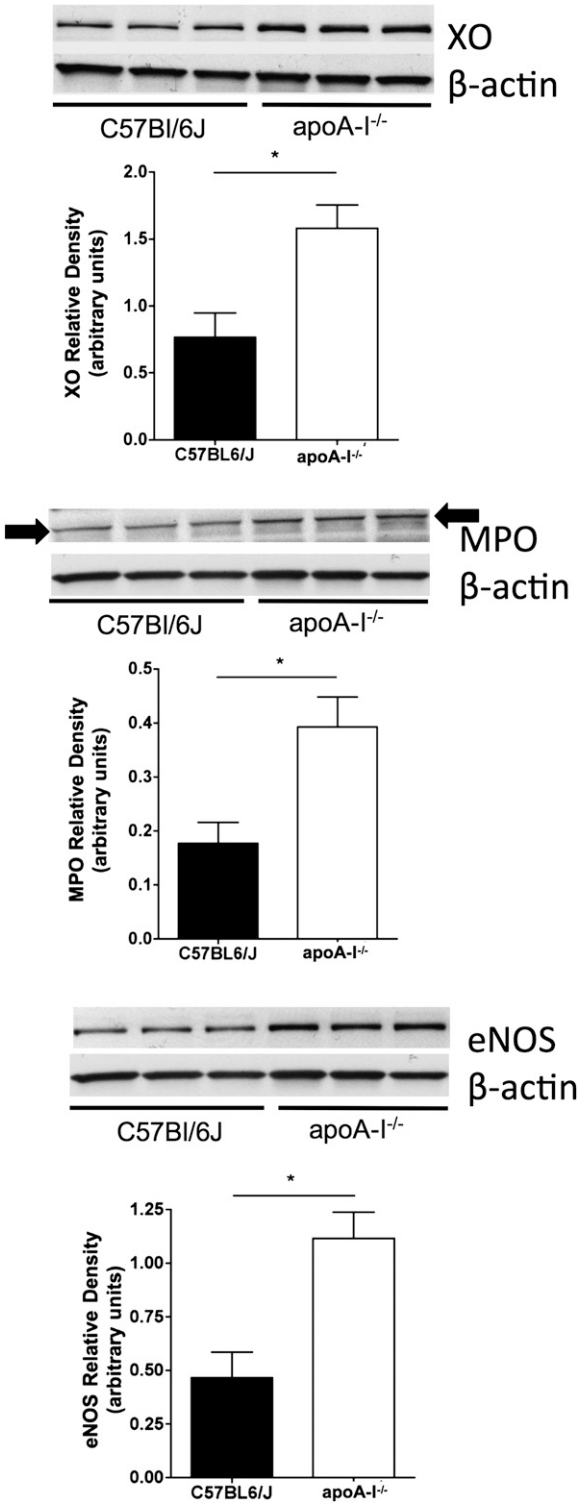

Fig. 8. Expression of oxidative enzymes in lungs. Autoradiograms showing relative band densities for immunoblots of (A) XO, (B) MPO, and (C) eNOS and corresponding β-actin as an internal loading control. Western blot analysis reveals that the expression of XO, MPO, and eNOS are all increased in *apoA-I*$^{-/-}$ mice compared with control mice (n = 3; *$P < 0.05$). apoA-I, apolipoprotein A-I; eNOS, endothelial nitric oxide synthase; MPO, myeloperoxidase; XO, xanthine oxidase.

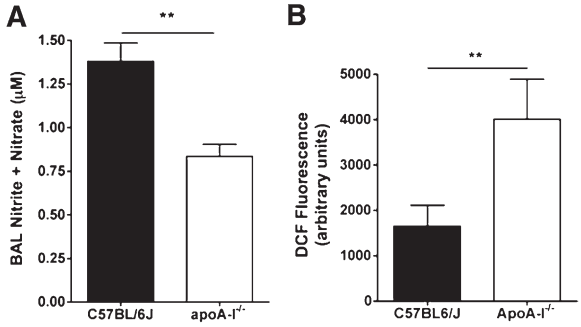

Fig. 9. BALF nitrite+nitrate and H_2DCF-dependent oxidants. A: Bar graphs showing that BALF isolated from *apoA-I*$^{-/-}$ mice (n = 7) contains lower concentrations of nitrite+nitrate than in BALF from C57BL/6J control mice (n = 7). B: Bar graph showing that BALF from *apoA-I*$^{-/-}$ mice contain higher concentrations of oxidants that react with H_2DCF to increase DCF fluorescence (n = 6–7; **$P < 0.01$). apoA-I, apolipoprotein A-I; BALF, bronchoalveolar lavage fluid.

can be achieved (unpublished observations). The composition of the inflammatory cells in the lungs of *apoA-I*$^{-/-}$ mice was predominantly neutrophils and leukocytes, whereas in C57BL/6J mice an occasion neutrophil was noted. Finally, although there was a tendency for leukocytes to be increased in BALF of *apoA-I*$^{-/-}$ mice, statistical analysis indicated that the difference between the two groups was not significant (Fig. 6).

Performing forced oscillatory techniques at different PEEP levels to determine R_N, G, and H has been shown to be a sensitive means of detecting differences in airway mechanics in response to increasing pressure between different strains of mice (19). We observed no differences in R_N between control and *apoA-I*$^{-/-}$ mice with increasing PEEP; however, G and H were increased in the *apoA-I*$^{-/-}$ mice throughout the entire PEEP range compared with C57BL/6J mice (Fig. 5). As R_N corresponds to central airways resistance, a change in R_N is expected only if the caliber of the conducting airways is significantly reduced. Thus, our data suggest that the increases in G and H represent inherent changes in the biophysical properties of very small airways or lung parenchyma in the *apoA-I*$^{-/-}$ mice. Again, this finding is consistent with histological data showing that lungs from *apoA-I*$^{-/-}$ mice contain greater levels of collagen than C57BL/6J mice (Fig. 6).

Immunofluorescence studies of the lung clearly indicated that the lungs of *apoA-I*$^{-/-}$ mice were under greater oxidative and nitrosative stress and inflammation than lungs of control mice. Lungs isolated from *apoA-I*$^{-/-}$ mice contained increased levels of 3-NT, an index of either peroxynitrite formation or nitrogen dioxide production (37–39) and 4-HNE Michael's adducts, an index of lipid peroxidation with respect to polyunsaturated fatty acid chain breakage (40), but not T15-autoantibodies, which detect the presence of oxidized phosphotidylcholine (41, 42). The marked increase in 4-HNE Michael's adducts is important in that, for the most part, it colocalized activation of TGFβ-1, which plays important roles in mesenchymal transition to generate fibroblasts and increase collagen deposition. Accordingly, our data begin to explain why

genetic loss of apoA-I, and possibly apoA-I dysfunction, increases collagen deposition and airway stiffening.

The lungs of *apoA-I*$^{-/-}$ mice are under greater oxidative stress than the lungs of control mice. Western blot analysis revealed that homogenates of *apoA-I*$^{-/-}$ lungs contained greater levels of XO, MPO, and eNOS than homogenates of control lungs (Fig. 8). Where cholesterol-rich diets (43) or ischemia/reperfusion (44, 45) are well recognized for increasing injury and, therefore, XO release from the liver, we observed that apoA-I deficiency induces a nearly 2-fold increase in XO expression in lung homogenates without apparent injury to the liver (data not shown). Our data indicate that pulmonary injury and subsequent XO generation and release can and does occur throughout the lung. Others have shown that the endothelium and epithelium are important sources of XO activity (46). For example, exposure of endothelial cells to hypoxia/reoxygenation increases both the conversion of XDH to XO and XO activity nearly 2-fold (47). Further, rhinovirus infection, a common mechanism for aggravating viral-induced asthma, increases superoxide anion generation in primary bronchial respiratory epithelial cells by proteolytic conversion of XDH into XO (48). Thus, several mechanisms exist to increase XO in pulmonary tissues. Likewise, increased MPO expression in the lungs of *apoA-I*$^{-/-}$ mice, presumably a result of neutrophil or leukocyte recruitment, is well recognized for increasing oxidative damage, injury, and tyrosine nitration in inflamed lungs. Finally, although one might assume that an increase in eNOS expression is protective because of increased potential for generating •NO, it has been shown that overexpression of eNOS in atherogenic mice actually increases lesion formation (49). Thus, while an increase in eNOS should be protective, the fact that lungs of *apoA-I*$^{-/-}$ mice are subjected to increased states of oxidative stress and inflammation suggests that pulmonary eNOS in *apoA-I*$^{-/-}$ mice might be uncoupled. Data supporting this notion are the decreased nitrite+nitrate concentrations in BALF in *apoA-I*$^{-/-}$ mice, the marked increases in 3-NT and 4-HNE Michael's adducts that colocalize with TGFβ-1 in the lungs of *apoA-I*$^{-/-}$ mice (Fig. 7), and ultimately, the marked increase in DCF-detectable oxidants in the BALF isolated from *apoA-I*$^{-/-}$ mice (Fig. 9). Quantification of free and esterified F2-isoprostanes in lung homogenates suggest that genetic loss of apoA-I increases the formation of F2-isoprostanes by 20–52% over and above the levels in C57BL/6J mice (data not shown). Numerous studies in other systems indicate that such conditions are a common prescription for uncoupled eNOS activity, a potential mechanism that will be examined in greater detail in future studies.

CONCLUSION

Our studies demonstrate that apoA-I plays an important protective role in preventing pulmonary inflammation, impaired vasodilatation, and increased airway hyperresponsiveness. Loss of apoA-I and its associated anti-inflammatory and anti-atherogenic properties has a profound and severe negative impact on the lung with respect to vascular function and airway physiology. Additional studies aimed at determining how apoA-I prevents inflammation and oxidative stress in the lung should reveal new insight into the cellular mechanisms by which apoA-I protects the lung.

The authors wish to thank Maria Zaidi for technical assistance.

REFERENCES

1. Bates, S. R., J. Q. Tao, H. L. Collins, O. L. Francone, and G. H. Rothblat. 2005. Pulmonary abnormalities due to ABCA1 deficiency in mice. *Am. J. Physiol. Lung Cell. Mol. Physiol.* **289:** L980–L989.
2. Yuditskaya, S., A. Tumblin, G. T. Hoehn, G. Wang, S. K. Drake, X. Xu, S. Ying, A. H. Chi, A. T. Remaley, R. F. Shen, et al. 2009. Proteomic identification of altered apolipoprotein patterns in pulmonary hypertension and vasculopathy of sickle cell disease. *Blood.* **113:** 1122–1128.
3. Otera, H., T. Ishida, T. Nishiuma, K. Kobayashi, Y. Kotani, T. Yasuda, R. K. Kundu, T. Quertermous, K. Hirata, and Y. Nishimura. 2009. Targeted inactivation of endothelial lipase attenuates lung allergic inflammation through raising plasma HDL level and inhibiting eosinophil infiltration. *Am. J. Physiol. Lung Cell. Mol. Physiol.* **296:** L594–L602.
4. Ansell, B. J., G. C. Fonarow, and A. M. Fogelman. 2006. High-density lipoprotein: is it always atheroprotective? *Curr. Atheroscler. Rep.* **8:** 405–411.
5. Ansell, B. J., M. Navab, S. Hama, N. Kamranpour, G. Fonarow, G. Hough, S. Rahmani, R. Mottahedeh, R. Dave, S. T. Reddy, et al. 2003. Inflammatory/antiinflammatory properties of high-density lipoprotein distinguish patients from control subjects better than high-density lipoprotein cholesterol levels and are favorably affected by simvastatin treatment. *Circulation.* **108:** 2751–2756.
6. Nicholls, S. J., L. Zheng, and S. L. Hazen. 2005. Formation of dysfunctional high-density lipoprotein by myeloperoxidase. *Trends Cardiovasc. Med.* **15:** 212–219.
7. Watanabe, J., K. J. Chou, J. C. Liao, Y. Miao, H. H. Meng, H. Ge, V. Grijalva, S. Hama, K. Kozak, G. Buga, et al. 2007. Differential association of hemoglobin with proinflammatory high density lipoproteins in atherogenic/hyperlipidemic mice. A novel biomarker of atherosclerosis. *J. Biol. Chem.* **282:** 23698–23707.
8. Van Lenten, B. J., S. Y. Hama, F. C. de Beer, D. M. Stafforini, T. M. McIntyre, S. M. Prescott, B. N. La Du, A. M. Fogelman, and M. Navab. 1995. Anti-inflammatory HDL becomes pro-inflammatory during the acute phase response. Loss of protective effect of HDL against LDL oxidation in aortic wall cell cocultures. *J. Clin. Invest.* **96:** 2758–2767.
9. Ohno, I., Y. Nitta, K. Yamauchi, H. Hoshi, M. Honma, K. Woolley, P. O'Byrne, G. Tamura, M. Jordana, and K. Shirato. 1996. Transforming growth factor beta 1 (TGF beta 1) gene expression by eosinophils in asthmatic airway inflammation. *Am. J. Respir. Cell Mol. Biol.* **15:** 404–409.
10. Minshall, E. M., D. Y. Leung, R. J. Martin, Y. L. Song, L. Cameron, P. Ernst, and Q. Hamid. 1997. Eosinophil-associated TGF-beta1 mRNA expression and airways fibrosis in bronchial asthma. *Am. J. Respir. Cell Mol. Biol.* **17:** 326–333.
11. Smith, L. J., M. Shamsuddin, P. H. Sporn, M. Denenberg, and J. Anderson. 1997. Reduced superoxide dismutase in lung cells of patients with asthma. *Free Radic. Biol. Med.* **22:** 1301–1307.
12. De Sanctis, G. T., J. A. MacLean, K. Hamada, S. Mehta, J. A. Scott, A. Jiao, C. N. Yandava, L. Kobzik, W. W. Wolyniec, A. J. Fabian, et al. 1999. Contribution of nitric oxide synthases 1, 2, and 3 to airway hyperresponsiveness and inflammation in a murine model of asthma. *J. Exp. Med.* **189:** 1621–1630.
13. Onufrak, S., J. Abramson, and V. Vaccarino. 2007. Adult-onset asthma is associated with increased carotid atherosclerosis among women in the Atherosclerosis Risk in Communities (ARIC) study. *Atherosclerosis.* **195:** 129–137.

14. Ou, J., J. Wang, H. Xu, Z. Ou, M. G. Sorci-Thomas, D. W. Jones, P. Signorino, J. C. Densmore, S. Kaul, K. T. Oldham, et al. 2005. Effects of D-4F on vasodilation and vessel wall thickness in hypercholesterolemic LDL receptor-null and LDL receptor/apolipoprotein A-I double-knockout mice on Western diet. *Circ. Res.* **97:** 1190–1197.
15. Aviram, M., S. Billecke, R. Sorenson, C. Bisgaier, R. Newton, M. Rosenblat, J. Erogul, C. Hsu, C. Dunlop, and B. La Du. 1998. Paraoxonase active site required for protection against LDL oxidation involves its free sulfhydryl group and is different from that required for its arylesterase/paraoxonase activities: selective action of human paraoxonase allozymes Q and R. *Arterioscler. Thromb. Vasc. Biol.* **18:** 1617–1624.
16. Ou, Z., J. Ou, A. W. Ackerman, K. T. Oldham, and K. A. Pritchard, Jr. 2003. L-4F, an apolipoprotein A-1 mimetic, restores nitric oxide and superoxide anion balance in low-density lipoprotein-treated endothelial cells. *Circulation.* **107:** 1520–1524.
17. Braman, R. S., and S. A. Hendrix. 1989. Nanogram nitrite and nitrate determination in environmental and biological materials by vanadium (III) reduction with chemiluminescence detection. *Anal. Chem.* **61:** 2715–2718.
18. Konduri, G. G., I. Bakhutashvili, A. Eis, and K. Pritchard, Jr. 2007. Oxidant stress from uncoupled nitric oxide synthase impairs vasodilation in fetal lambs with persistent pulmonary hypertension. *Am. J. Physiol. Heart Circ. Physiol.* **292:** H1812–H1820.
19. Gomes, R. F., X. Shen, R. Ramchandani, R. S. Tepper, and J. H. Bates. 2000. Comparative respiratory system mechanics in rodents. *J. Appl. Physiol.* **89:** 908–916.
20. Hantos, Z., A. Adamicza, E. Govaerts, and B. Daroczy. 1992. Mechanical impedances of lungs and chest wall in the cat. *J. Appl. Physiol.* **73:** 427–433.
21. Tomioka, S., J. H. Bates, and C. G. Irvin. 2002. Airway and tissue mechanics in a murine model of asthma: alveolar capsule vs. forced oscillations. *J. Appl. Physiol.* **93:** 263–270.
22. Finotto, S., M. F. Neurath, J. N. Glickman, S. Qin, H. A. Lehr, F. H. Green, K. Ackerman, K. Haley, P. R. Galle, S. J. Szabo, et al. 2002. Development of spontaneous airway changes consistent with human asthma in mice lacking T-bet. *Science.* **295:** 336–338.
23. Ingenito, E. P., S. H. Loring, M. L. Moy, S. J. Mentzer, S. J. Swanson, A. Hunsaker, C. C. McKee, and J. J. Reilly. 2001. Comparison of physiological and radiological screening for lung volume reduction surgery. *Am. J. Respir. Crit. Care Med.* **163:** 1068–1073.
24. Pritchard, K. A., Jr., J. Ou, Z. Ou, Y. Shi, J. P. Franciosi, P. Signorino, S. Kaul, C. Ackland-Berglund, K. Witte, S. Holzhauer, et al. 2004. Hypoxia-induced acute lung injury in murine models of sickle cell disease. *Am. J. Physiol. Lung Cell. Mol. Physiol.* **286:** L705–L714.
25. Weihrauch, D., H. Xu, Y. Shi, J. Wang, J. Brien, D. W. Jones, S. Kaul, R. A. Komorowski, M. E. Csuka, K. T. Oldham, et al. 2007. Effects of D-4F on vasodilation, oxidative stress, angiostatin, myocardial inflammation and angiogenic potential in Tight-skin mice. *Am. J. Physiol. Heart Circ. Physiol.* **293:** H1432–H1441.
26. Navab, M., S. Y. Hama, G. P. Hough, G. Subbanagounder, S. T. Reddy, and A. M. Fogelman. 2001. A cell-free assay for detecting HDL that is dysfunctional in preventing the formation of or inactivating oxidized phospholipids. *J. Lipid Res.* **42:** 1308–1317.
27. Williamson, R., D. Lee, J. Hagaman, and N. Maeda. 1992. Marked reduction of high density lipoprotein cholesterol in mice genetically modified to lack apolipoprotein A-I. *Proc. Natl. Acad. Sci. USA.* **89:** 7134–7138.
28. Plump, A. S., N. Azrolan, H. Odaka, L. Wu, X. Jiang, A. Tall, S. Eisenberg, and J. L. Breslow. 1997. ApoA-I knockout mice: characterization of HDL metabolism in homozygotes and identification of a post-RNA mechanism of apoA-I up-regulation in heterozygotes. *J. Lipid Res.* **38:** 1033–1047.
29. Nandedkar, S. D., T. R. Feroah, W. Hutchins, D. Weihrauch, K. S. Konduri, J. Wang, R. C. Strunk, M. R. DeBaun, C. A. Hillery, and K. A. Pritchard. 2008. Histopathology of experimentally induced asthma in a murine model of sickle cell disease. *Blood.* **112:** 2529–2538.
30. Navab, M., G. M. Anantharamaiah, S. Hama, D. W. Garber, M. Chaddha, G. Hough, R. Lallone, and A. M. Fogelman. 2002. Oral administration of an Apo A-I mimetic peptide synthesized from D-amino acids dramatically reduces atherosclerosis in mice independent of plasma cholesterol. *Circulation.* **105:** 290–292.
31. Ou, J., Z. Ou, D. W. Jones, S. Holzhauer, O. A. Hatoum, A. W. Ackerman, D. W. Weihrauch, D. D. Gutterman, K. Guice, K. T. Oldham, et al. 2003. L-4F, an apolipoprotein A-1 mimetic, dramatically improves vasodilation in hypercholesterolemia and sickle cell disease. *Circulation.* **107:** 2337–2341.
32. Feingold, K. R., R. A. Memon, A. H. Moser, and C. Grunfeld. 1998. Paraoxonase activity in the serum and hepatic mRNA levels decrease during the acute phase response. *Atherosclerosis.* **139:** 307–315.
33. Peterson, T. E., V. Poppa, H. Ueba, A. Wu, C. Yan, and B. C. Berk. 1999. Opposing effects of reactive oxygen species and cholesterol on endothelial nitric oxide synthase and endothelial cell caveolae. *Circ. Res.* **85:** 29–37.
34. Hirai, T., and J. H. Bates. 2001. Effects of deep inspiration on bronchoconstriction in the rat. *Respir. Physiol.* **127:** 201–215.
35. Hirai, T., K. A. McKeown, R. F. Gomes, and J. H. Bates. 1999. Effects of lung volume on lung and chest wall mechanics in rats. *J. Appl. Physiol.* **86:** 16–21.
36. Irvin, C. G., and J. H. Bates. 2003. Measuring the lung function in the mouse: the challenge of size. *Respir. Res.* **4:** 4.
37. Beckman, J. S., and W. H. Koppenol. 1996. Nitric oxide, superoxide, and peroxynitrite: the good, the bad, and ugly. *Am. J. Physiol.* **271:** C1424–C1437.
38. Halliwell, B. 1997. What nitrates tyrosine? Is nitrotyrosine specific as a biomarker of peroxynitrite formation in vivo? *FEBS Lett.* **411:** 157–160.
39. Eiserich, J. P., M. Hristova, C. E. Cross, A. D. Jones, B. A. Freeman, B. Halliwell, and A. van der Vliet. 1998. Formation of nitric oxide-derived inflammatory oxidants by myeloperoxidase in neutrophils. *Nature.* **391:** 393–397.
40. Liu, J., A. Ormsby, N. Oja-Tebbe, and P. J. Pagano. 2004. Gene transfer of NAD(P)H oxidase inhibitor to the vascular adventitia attenuates medial smooth muscle hypertrophy. *Circ. Res.* **95:** 587–594.
41. Binder, C. J., K. Hartvigsen, M. K. Chang, M. Miller, D. Broide, W. Palinski, L. K. Curtiss, M. Corr, and J. L. Witztum. 2004. IL-5 links adaptive and natural immunity specific for epitopes of oxidized LDL and protects from atherosclerosis. *J. Clin. Invest.* **114:** 427–437.
42. Daugherty, A., D. L. Rateri, and V. L. King. 2004. IL-5 links adaptive and natural immunity in reducing atherosclerotic disease. *J. Clin. Invest.* **114:** 317–319.
43. White, C. R., V. Darley-Usmar, W. R. Berrington, M. McAdams, J. Z. Gore, J. A. Thompson, D. A. Parks, M. M. Tarpey, and B. A. Freeman. 1996. Circulating plasma xanthine oxidase contributes to vascular dysfunction in hypercholesterolemic rabbits. *Proc. Natl. Acad. Sci. USA.* **93:** 8745–8749.
44. Aslan, M., T. M. Ryan, B. Adler, T. M. Townes, D. A. Parks, J. A. Thompson, A. Tousson, M. T. Gladwin, R. P. Patel, M. M. Tarpey, et al. 2001. Oxygen radical inhibition of nitric oxide-dependent vascular function in sickle cell disease. *Proc. Natl. Acad. Sci. USA.* **98:** 15215–15220.
45. Aslan, M., and B. A. Freeman. 2004. Oxidant-mediated impairment of nitric oxide signaling in sickle cell disease–mechanisms and consequences. *Cell Mol. Biol. (Noisy-le-grand).* **50:** 95–105.
46. Bellocq, A., E. Azoulay, S. Marullo, A. Flahault, B. Fouqueray, C. Philippe, J. Cadranel, and L. Baud. 1999. Reactive oxygen and nitrogen intermediates increase transforming growth factor-beta1 release from human epithelial alveolar cells through two different mechanisms. *Am. J. Respir. Cell Mol. Biol.* **21:** 128–136.
47. Poss, W. B., T. P. Hueckstead, P. C. Panus, B. A. Freeman, and J. R. Hoidal. 1996. Regulation of xanthine dehydrogenase and xanthine oxidase activity by hypoxia. *Am. J. Physiol.* **270:** L941–L946.
48. Papi, A., M. Contoli, P. Gasparini, L. Bristot, M. R. Edwards, M. Chicca, M. Leis, A. Ciaccia, G. Caramori, S. L. Johnston, et al. 2008. Role of xanthine oxidase activation and reduced glutathione depletion in rhinovirus induction of inflammation in respiratory epithelial cells. *J. Biol. Chem.* **283:** 28595–28606.
49. Ozaki, M., S. Kawashima, T. Yamashita, T. Hirase, M. Namiki, N. Inoue, K. Hirata, H. Yasui, H. Sakurai, Y. Yoshida, et al. 2002. Overexpression of endothelial nitric oxide synthase accelerates atherosclerotic lesion formation in apoE-deficient mice. *J. Clin. Invest.* **110:** 331–340.